MATERIALS SCIENCE

Programmable and scalable transfer printing with high reliability and efficiency for flexible inorganic electronics

Chengjun Wang[1], Changhong Linghu[1], Shuang Nie[1], Chenglong Li[1], Qianjin Lei[1], Xiang Tao[2], Yinjia Zeng[1], Yipu Du[1], Shun Zhang[1], Kaixin Yu[1], Hao Jin[2], Weiqiu Chen[1], Jizhou Song[1]*

Transfer printing that enables heterogeneous integration of materials in desired layouts offers unprecedented opportunities for developing high-performance unconventional electronic systems. However, large-area integration of ultrathin and delicate functional micro-objects with high yields in a programmable fashion still remains as a great challenge. Here, we present a simple, cost-effective, yet robust transfer printing technique via a shape-conformal stamp with actively actuated surface microstructures for programmable and scalable transfer printing with high reliability and efficiency. The shape-conformal stamp features the polymeric backing and commercially available adhesive layer with embedded expandable microspheres. Upon external thermal stimuli, the embedded microspheres expand to form surface microstructures and yield weak adhesion for reliable release. Systematic experimental and computational studies reveal the fundamental aspects of the extraordinary adhesion switchability of stamp. Demonstrations of this protocol in deterministic assemblies of diverse challenging inorganic micro-objects illustrate its extraordinary capabilities in transfer printing for developing high-performance flexible inorganic electronics.

INTRODUCTION

Advances in high-performance inorganic electronics with flexibility and stretchability have enabled novel applications in bio-integrated health-monitoring devices (1–4), curvilinear electronics (5), deformable displays (6, 7), etc. A crucial step in manufacturing these unconventional electronic systems relies heavily on heterogeneous integration of inorganic materials with soft polymeric substrates, which requires the transfer of tiny, ultrathin, and delicate functional components (i.e., inks) from their fabricated rigid wafers to target soft polymeric substrates. However, the well-established pick-and-place techniques (i.e., single-ejector needle or vacuum nozzles) are unable to meet this stringent requirement (8, 9). As an emerging manufacturing technique, transfer printing enables the assembly of multiscale and classes of materials on demand using a soft stamp and has been demonstrated to be a promising solution (10–17). A reliable transfer printing critically depends on the switch of stamp/ink interfacial adhesion strength from the strong state for successful retrieval to the weak state for easy release of inks. Various strategies based on tunable dry adhesive have been proposed to develop transfer printing such as kinetically controlled transfer printing (14) and gecko- or aphid-inspired transfer printing (15–17). Among all these schemes, stamps with surface engineered microstructures show the unique capability in achieving weak adhesion for releasing, which makes them suitable in transfer printing of tiny, ultrathin, and delicate inks with high yields.

In addition to the large adhesion switchability, the manipulation of stamp/ink interfacial adhesion in a programmable and scalable manner to enable a reliable selective transfer printing is highly desired in practical applications, where variable pitch spacing or densities of inks across a large area on receiver substrates are needed

(12). For example, the well-established microscale, ultrathin bare dies such as inorganic light-emitting diodes (LEDs) or photodiodes can be prepared densely on fabricated source wafers for cost savings and then transfer printed onto target substrates with desired layouts in a relatively sparse form for on-demand usage, e.g., micro-LED displays (5, 6, 18–20) and wearable optoelectronic sensors (1, 2, 12, 21). A few previous attempts including pneumatic or stimuli-response material–based actively actuated stamps (15, 16, 22, 23) and passively selective stamps with predefined elastomeric posts (12, 17, 19) have presented valuable proof of this concept. However, each method has its own drawbacks in terms of individually addressable ability, adhesion switchability, or scalability. Laser-assisted transfer printing due to the rapid and localized heat delivery by the laser is considered as the most promising solution to overcome the above drawbacks and, thus, to ensure a reliable selective transfer printing. Typically, two laser-assisted transfer printing strategies have been used to transfer the functional inks. One is laser-induced forward transfer process, which relies on thermal-induced mechanical mismatch or the irradiation-induced damage of a surface thin layer to release and print inks, at an undesired high laser power (24–27). The other is to construct thermal-induced shape change for tuning adhesion upon absorbed heat from the laser despite the slow response in thermal-sensitive material and sophisticated preparation of stamp (15, 20, 28, 29). These protocols are effective to assemble diverse materials in various structural layouts. However, the programmable and scalable transfer printing of tiny, ultrathin, and delicate inks in a high-throughput manner still remains as a difficult challenge.

Here, we report a simple, cost-effective, yet robust transfer printing technique with high reliability and efficiency that combines large-area manufacturing capability in a high-throughput manner and programmable transfer printing of tiny, ultrathin, and delicate electronic or optoelectronic components on demand. The prototype uses the shape-conformal thin sheet with embedded thermal expandable microspheres in its adhesive layer to serve as stamp instead of traditional thick elastomeric stamp for transfer printing. Initially, the small size of embedded expandable microspheres can ensure a flat

[1]Department of Engineering Mechanics, Soft Matter Research Center, and Key Laboratory of Soft Machines and Smart Devices of Zhejiang Province, Zhejiang University, Hangzhou 310027, China. [2]College of Information Science and Electronic Engineering, Zhejiang University, Hangzhou 310027, China.
*Corresponding author. Email: jzsong@zju.edu.cn

topography and a negligible effect on strong adhesion of the adhesive layer. Upon exposure to external thermal stimuli, i.e., 90°C, the marked volume expansion of microspheres rapidly induces the surface hierarchical microstructures and therefore ensures extremely weak adhesion for reliable release of inks attached on the stamp onto various receiver substrates. Through a homemade programmable and highly localized laser heating system with the automated translational stage or scanning laser beam functionality, the selective and scalable transfer printing capability of this protocol is easily realized in a highly efficient way. Systematic experimental and computational studies reveal the underlying mechanism of the extraordinary abilities of the thermal releasable adhesive with embedded expandable microspheres with the gentle processing laser power to achieve complete thermal stimuli to expandable microspheres and, simultaneously, without any thermal damages to transferred functional objects. Demonstrations of this protocol in programmable transfer printing of Si nanomembranes, Si nanomembrane–based photodiodes, polyimide-based thin film sensors in a large-area manner, as well as the fabrication of ultrathin inorganic LED array–based flexible display, illustrate its robust capabilities in transfer printing of tiny, ultrathin, and delicate electronic or optoelectronic bare dies and its great potential in ultrathin flexible electronics manufacturing.

RESULTS

The construct of shape-conformal stamp toward high-reliability transfer printing

Figure 1A schematically illustrates the novel concept design to construct a shape-conformal stamp with large adhesion switchability and, therefore, high transfer printing yields. The strategy features a
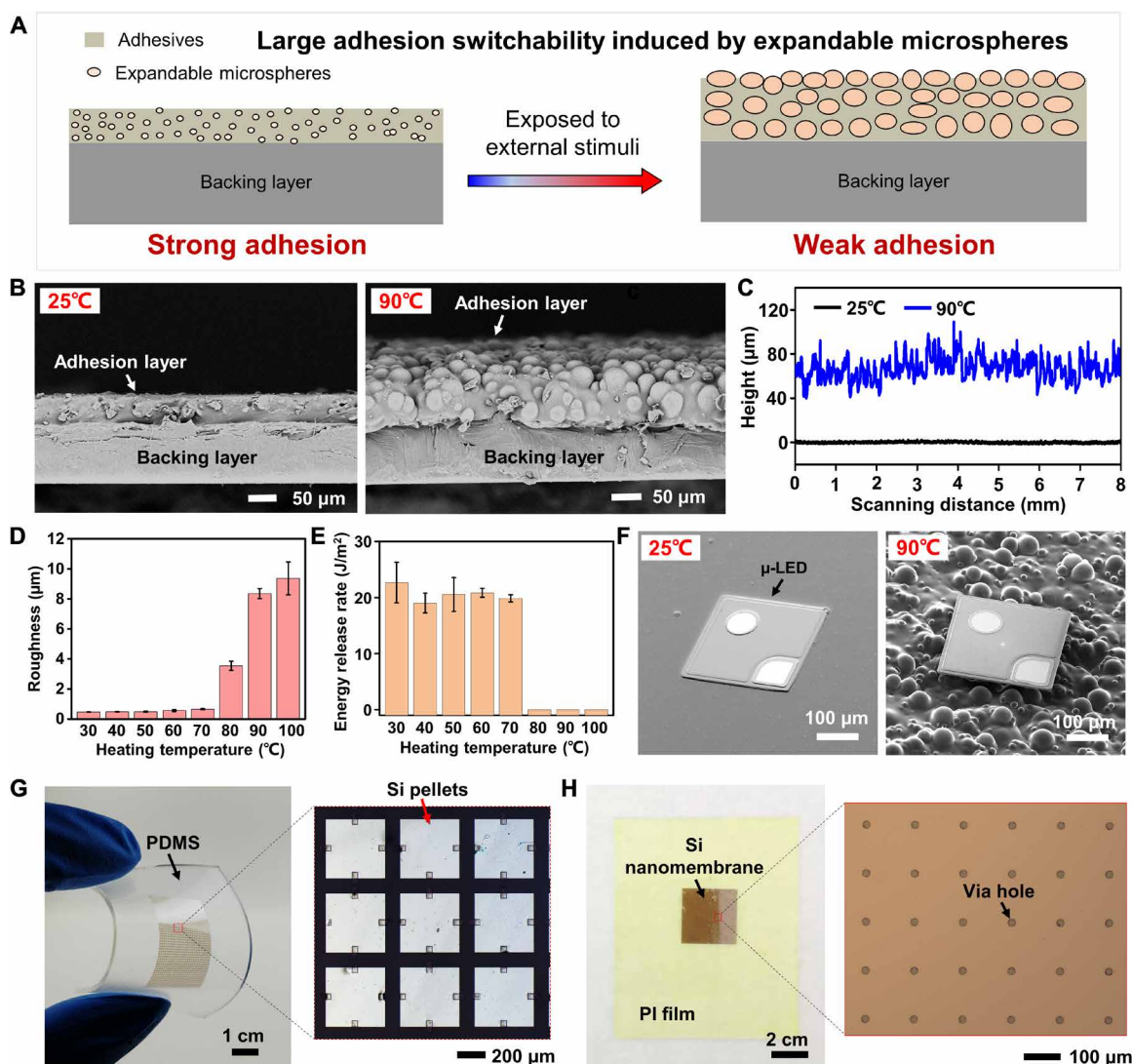
Fig. 1. The mechanism of shape-conformal stamp with large adhesion switchability and demonstrations for transfer printing of ultrathin Si nanomembranes. (**A**) Schematic illustration of the novel concept design to construct a shape-conformal stamp with large adhesion switchability. (**B**) SEM images and (**C**) corresponding profile of TRT stamp before and after heating on a hotplate. (**D**) The measured surface roughness of the TRT stamp and (**E**) energy release rate of the TRT stamp with the glass slide after being uniformly heated on a hotplate at various temperatures. (**F**) SEM images of the ultrathin, inorganic μ-LED (285 μm by 285 μm by 4.6 μm) on the TRT stamp before and after heating on a hotplate, respectively. (**G**) Optical image of transfer-printed ultrathin Si pellets (400 μm by 400 μm by 200 nm) on the PDMS substrate under bending deformation. (**H**) Optical image of large-area Si nanomembrane (2 cm by 2 cm by 3 μm) transfer printed onto the PI substrate. Photo credit: C.W. and C.Lin., Zhejiang University.

shape-conformal bilayer thin sheet consisting of the polymeric backing layer and commercially available adhesive matrix with embedded expandable microspheres to serve as a stamp. Initially, the small size of expandable microspheres can ensure a flat topography and, thus, a negligible effect on adhesion strength of the strong adhesive layer. The extremely large volume expansion of microspheres upon external stimuli (e.g., heat and hydro) can rapidly induce hierarchical microstructures on the surface of the adhesive layer and decrease the adhesion strength markedly. It is noted that the expandable microspheres can be easily prepared through large volume change of liquid-vapor transition of liquids entrapped inside the elastomeric matrixes (30) or thermoplastic polymer shells by suspension polymerization method (31), as well as hydrogel particles from absorbed water (32, 33), etc. Here, to illustrate the working mechanism of the proposed scheme, the commercially available thermal release tape (TRT; no. 3195, Nitto) with embedded thermally expandable microspheres in its adhesive is chosen as an example. The thermally expandable microspheres with hydrocarbons encapsulated inside thermoplastic polymer shells were first prepared and then randomly and uniformly dispersed into the adhesive layer of TRT in both depth and width directions. The liquid-vapor transition of inner hydrocarbons and softening of thermoplastic polymer shells at a given temperature, i.e., 90°C, lead to large volume expansion of microspheres from around 10 to 45 μm in diameter without any gas bubbles generated (34). The observed microscopic topography and measured surface profile (step profilometer, Bruker DektakXT, GER) of the TRT stamp before and after heating on a hotplate at 90°C (Fig. 1, B and C) show the simple yet robust way to actively form visible surface hierarchical microstructures on a shape-conformal stamp through external thermal stimuli.

Furthermore, quantitative studies of the surface roughness R_a (arithmetical mean deviation of the profile) and energy release rate (or adhesion strength) of the TRT stamp at various given temperatures are also conducted (Fig. 1, D and E). The representative peeling force of the TRT stamp with glass slide as a function of displacement is given in fig. S1A. It is observed that both the surface roughness R_a and adhesion strength of the TRT stamp have abrupt changes at the same temperature, i.e., 80°C, which implies the occurrence of liquid-vapor phase transition. The similar dependences of the surface roughness and adhesion strength on the temperature increase validate that the extremely weak adhesion of the TRT stamp at 90°C is attributed to the large increase in surface roughness, which indicates the importance of surface microstructures for adhesion modulation. The excellent adhesion switchability of the TRT stamp is also applicable to other commonly used materials for flexible inorganic electronics such as polished silicon and polyimide film, as shown in fig. S1B. It should be pointed out that the adhesion switchability of the TRT stamp with in situ actively controllable microstructures greatly surpasses those elastomeric stamps with the predefined surface relief microstructures in most previous designs (15, 17) since it can ensure very large contact area and strong adhesion between the stamp and inks for reliable retrieval and, simultaneously, extremely small contact area and weak adhesion for successful release of inks to various receiver substrates via external thermal stimuli. We measured the surface adhesion strength of flat polydimethylsiloxane (PDMS) stamp (the commonly used soft elastomeric stamp currently for assemblies of flexible inorganic electronics) with polished silicon wafer, as shown in fig. S1C. It is shown that the strong adhesion for picking at 25°C is 22.68 J/m^2 (fig. S1B) for the TRT stamp

and 3.97 J/m^2 at 2000 μm/s peeling speed for the PDMS stamp, while the weak adhesion for releasing is too small to measure with the load cell at 90°C for the TRT stamp (less than 0.2 J/m^2 based on the minimum force of the load cell measured, i.e., 2 mN) and 2.56 J/m^2 at 50 μm/s peeling speed for the PDMS stamp. Figure 1F shows the scanning electron microscopy (SEM) images of microscale inorganic LED chip (285 μm by 285 μm by 4.6 μm) adhered on the TRT stamp before and after heating on a hotplate at 90°C, which illustrates the excellent strong and weak adhesion switchability of the TRT stamp to ultrathin inks via actively actuated surface microstructures.

To demonstrate the extraordinary ability of the TRT stamp in transfer printing of tiny, ultrathin, and delicate inks, a 64 by 40 array of silicon nanomembrane pellets with in-plane size of 400 μm by 400 μm and thickness of 200 nm was fabricated on a silicon-on-insulator (SOI) wafer and then completely picked up using the TRT stamp. The detailed fabrication process of Si pellets is shown in fig. S2A. Upon heating on a hotplate at 90°C, the surface hierarchical microstructures of the TRT stamp are rapidly formed because of the large volume change of expandable microspheres and dynamically drive Si nanomembranes into the weak adhesion state to the TRT stamp for reliable release. Figure 1G shows the optical image of printed Si nanomembrane pellets of 64 by 40 array on a PDMS slab in deformable form. The optical images of the Si nanomembrane array on fabricated SOI wafer, TRT stamp, and PDMS receiver substrate are shown in fig. S2B. For thinner films with a thickness of tens of nanometers (or even thinner), this technique is not applicable because of the potential mechanical damage risks during the thermal expansion of stamp. Besides, the extraordinary adhesion switchability of the TRT stamp makes it applicable to transfer large-area Si nanomembrane (20 mm by 20 mm by 3 μm) from the rigid SOI wafer to flexible polyimide substrate (Fig. 1H), which is of great importance to the manufacturing of emerging, high-performance heterojunction hybrid electronics (35).

It is pointed out that, although the TRT has been reported previously to transfer various functional materials (36–38) onto unconventional substrates, the illustration of its underlying mechanism from the perspective of actively controllable surface microstructures and demonstrations of its extraordinary capability in transfer printing of tiny, ultrathin, and delicate inks are uncovered, which provides notable insights into constructing a shape-conformal stamp toward high-reliability transfer printing. In addition, the actively controllable surface microstructures of the TRT stamp through in situ thermally expandable microspheres ensures the strong adhesion for reliable retrieval and weak adhesion for successful releasing of inks simultaneously, which holds substantial advantages over those with predefined microstructures from sophisticated design and complex manufacturing. These unique properties of the TRT stamp facilitate a good opportunity for laser-assisted programmable and scalable transfer printing of tiny, ultrathin, and delicate inks with high efficiency and yields, which still remains a grand challenge to the large-area and cost-effective manufacturing of high-performance unconventional electronic systems.

Programmable and scalable transfer printing via automated translational stage

Benefitting from the rapid and extraordinary adhesion switchability of the TRT stamp upon external thermal stimuli, a promising transfer printing technique toward high yields and efficiency in a programmable and scalable manner can be easily developed, by combining

the merits of digitally controllable and highly localized laser heating system. Figure 2A schematically illustrates the basic apparatus to construct the laser-assisted programmable transfer printing prototype, which consists of a digitally controllable laser system for rapid and localized heat delivery to induce the TRT stamp into weak adhesion state, an optical microscopy for in situ monitoring, and the automated translational stage for the precise position and alignment between inks and laser in a programmable manner. Figure S3 shows the optical image of the homemade programmable transfer printing prototype with a laser beam of 808-nm wavelength and 350-μm diameter of light spot guided by an optical fiber. To perform the programmable transfer printing, the arrayed inks fabricated on source wafers are first picked up using the TRT stamp and then selectively printed onto various receiver substrates with desired patterns after locally irradiating and releasing adhesion of the TRT stamp where individual ink to be transferred is occupied. One of the critical challenges
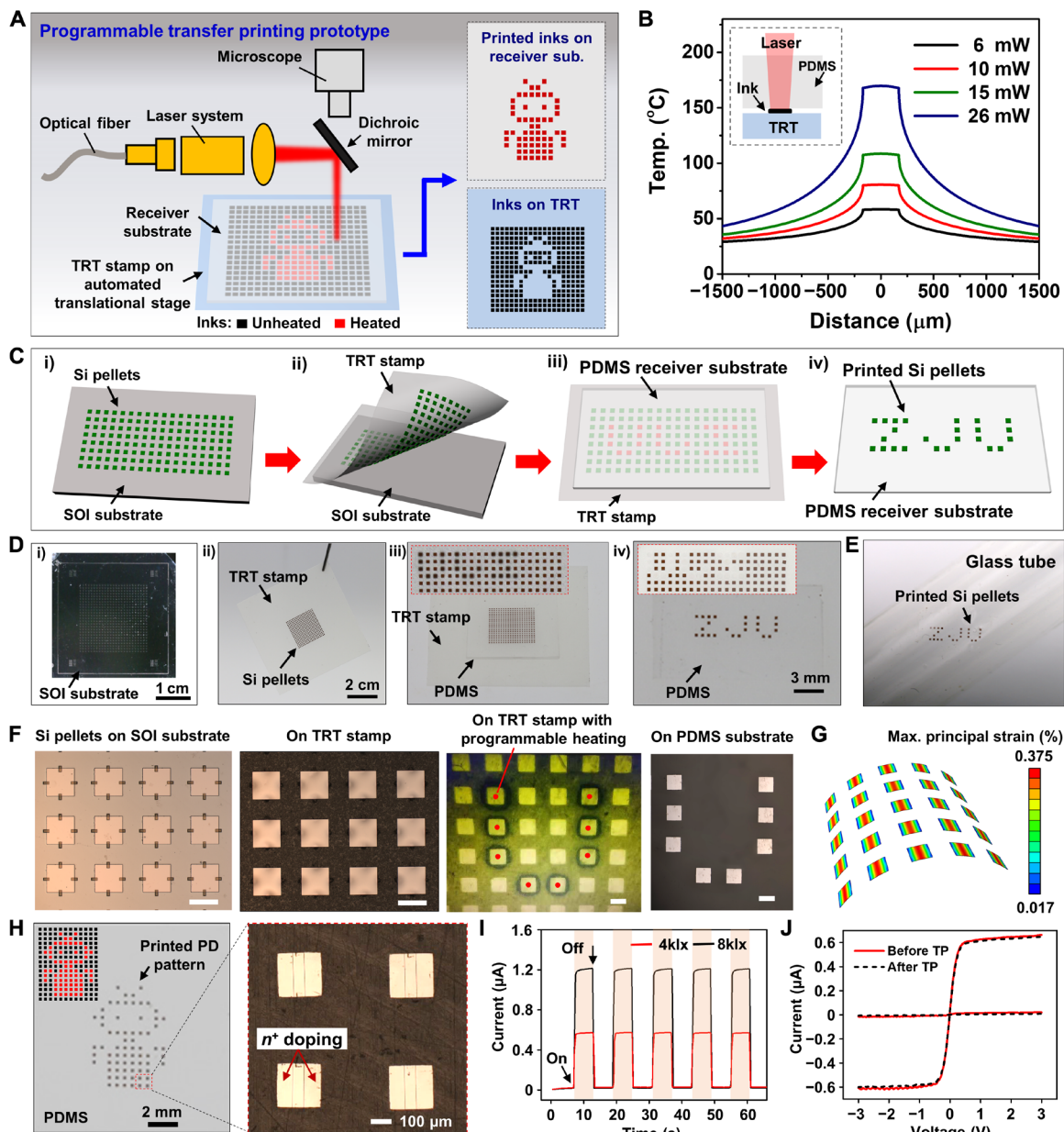
Fig. 2. Programmable transfer printing of Si nanomembranes and Si nanomembrane–based photodetectors. (**A**) Schematic prototype of the laser-assisted programmable transfer printing system via automated translational stage. (**B**) Temperature increase at the interface of the TRT stamp and Si ink under various laser powers. (**C**) Schematic illustration of the programmable transfer printing process: (i) preparing Si pellets on an SOI wafer, (ii) picking up Si pellets using TRT stamp, (iii) programmable heating of Si pellets, and (iv) printing Si pellets on PDMS substrate. (**D**) Optical images of the programmable transfer printing process. (**E**) The selectively printed Si pellets on an Ecoflex-coated glass tube. (**F**) The magnified microscopic images corresponding to (D). Scale bars, 350 μm. (**G**) Maximum principal strain distribution of Si pellets under the bending radius of 1.5 mm. (**H**) Selectively printed Si nanomembrane–based photodetectors with a robot-like pattern on PDMS substrate. (**I**) Dynamic response of photodetector at various given light intensities and (**J**) measured *I-V* curve of the photodetector before and after transfer printing on PDMS receiver substrate. Photo credit: C.W. and S.N., Zhejiang University.

in achieving the programmable transfer printing prototype is to choose the favorable laser power for adequate irradiation of the TRT stamp and, meanwhile, avoiding undesired performance degradation of functional inks due to temperature increase. To optimize a gentle laser power, a finite element model is established to determine the temperature field of the TRT stamp under various applied laser powers. As an illustrative example, here in the finite element analysis (FEA), Si pellet with a thickness of 3 μm is taken as the representative ink and a thin slab of PDMS (1 mm thick), due to its excellent optical transmission at the given laser wavelength for in situ monitoring and heat delivery, is chosen as the receiver substrate and laminated onto the TRT stamp with Si pellet inks. Thus, laser energy from the programmable laser system can directly transmit the PDMS receiver substrate and be absorbed sufficiently by the Si pellet to heat the TRT stamp into the weak adhesion state. The geometric model of FEA is schematically illustrated in fig. S4A. The temperature distributions at the interface of the TRT stamp and Si ink under various absorbed laser powers are investigated (Fig. 2B), and the contour of temperature increase at the laser power of 15 mW is given in fig. S4B. It is observed that a relatively low laser power of 15 mW at 800-ms duration can induce a desired temperature increase for activation of the TRT stamp into the weak adhesion state. In terms of the optical reflectivity and transmission loss of the Si pellet in practical applications, the applied laser power of the programmable laser system is required relatively higher than the absorbed laser power of Si pellet based on a simple theoretical evaluation (24), as described in the Supplementary Materials.

To demonstrate the programmable transfer printing capability, a 40 by 40 array of Si pellets (350 μm by 350 μm by 3 μm) was fabricated on an SOI wafer. Figure 2C shows the schematic images of the programmable transfer printing process, which involve (i) preparing Si inks on the SOI wafer, (ii) picking up Si inks from the SOI wafer using the TRT stamp, (iii) laminating a PDMS slab onto the TRT stamp as temporary receiver substrate and programmable irradiation of Si inks to be transferred via automated translational stage with one cycle of pulse input of localized laser (800-ms duration and applied power of 0.15 W), and (iv) separating the TRT stamp with PDMS to yield Si inks with predefined patterns on PDMS receiver substrates. Figure 2D shows the corresponding optical images of the programmable transfer printing process, where a simple "ZJU" pattern formed by discrete Si pellets was selectively transfer printed onto a slab of PDMS receiver substrate. It is noted that the patterns of selectively transfer-printed inks on the PDMS receiver substrate can be easily and digitally controlled into more complex patterns through external programmable design and also can be picked up again from the PDMS substrate with another TRT stamp and printed onto other types of target receiver substrates that are a little bit sticky through global heating. Figure 2E shows the ZJU pattern on an Ecoflex-coated curvilinear glass tube (diameter, 18 mm), which was transfer printed from the Si pellets of ZJU on the PDMS receiver substrate. For nonsticky substrates such as glass and silicon wafer, the high transfer yields may not be ensured since the surface force dominates the gravity and the releasing of the inks poses the central challenge. The corresponding microscopic images and measured surface roughness of the Si pellets on fabricated SOI wafer, TRT stamp before and after programmable heating, and PDMS receiver substrate are shown in Fig. 2F and fig. S5. No damage or surface roughness change as well as residual adhesive of the Si pellets due to the expansion of microspheres were observed during the transfer printing process. In addition,

the optimized laser power has little thermal disturbance to neighboring inks during programmable laser heating. The associated deformation and strain in the Si pellet array due to bending deformation of the TRT stamp for picking up inks from source wafers (Fig. 2C-ii) were also investigated by FEA. It is observed that the maximum principal strain in the Si pellet array is less than 0.375% after being wrapped around a glass rod with the radius of 1.5 mm (Fig. 2G), which is smaller than its fracture strain (~1%). These results demonstrate that the TRT stamp–based laser-assisted programmable and scalable transfer printing prototype via automated translational stage has promising ability in selective transfer printing of tiny, ultrathin, and delicate inks with high yields.

To quantify the effect of the laser-assisted programmable transfer printing on the performance of functional inks, a 39 by 39 array of Si photodetector was prepared on an SOI wafer. The Si photodetector was fabricated by selective doping to define two p-n junctions in a back-to-back configuration. The details of the fabrication process are schematically illustrated in fig. S6. The rapid response of the laser system and highly programmable capability of the automated translational stage make it convenient and efficient to achieve complex patterns, which is critical to the high assembly rate for the manufacturing of high-performance unconventional electronics. Figure 2H shows the optical image of selectively printed Si photodetectors with a complex robot-like pattern on the PDMS receiver substrate out of an array of 39 by 39. The schematic inset shows the programmable heating pattern of the inks, and the magnified image on its right hand shows the details of the Si photodetector including two back-to-back n-p dopant regions. The measured dynamic response of the photodetector with and without light illumination at two given light intensities and a 3-V bias is shown in Fig. 2I. The current versus voltage (I-V) characteristics of the Si photodetector are also measured before (on fabricated rigid SOI wafer) and after (on soft PDMS substrate) transfer printing (Fig. 2J). No notable performance degradation was observed after laser-assisted programmable transfer printing onto a soft PDMS substrate compared with those on an SOI wafer, which further verifies the extraordinary capability of the programmable transfer printing prototype in selective transfer of tiny, ultrathin, and delicate inks.

Programmable and scalable transfer printing via scanning laser beam functionality

To demonstrate the programmable and scalable capability of the TRT stamp toward large-area transfer printing of functional inks in a high-throughput manner, a homemade galvanometer mirror–based, digitally controllable laser system with scanning laser beam functionality is established (fig. S7). Since the commercially available TRT can absorb about half of the laser energy at the given laser wavelength of 1064 nm from the measured optical absorption spectrum (fig. S8A), to enhance the reliability of transfer printing and decrease the required laser power for heat delivery, a thin layer of black polyester thin film, which can fully absorb the laser power, is adhered onto the backside of the TRT stamp (fig. S8, B and C).

To perform the programmable and scalable transfer printing, a 25 by 28 array of strain sensor (400 μm by 400 μm by 8 μm) was fabricated on a rigid silicon wafer to serve as the representative inks for transfer printing (Fig. 3A). The fabrication process is schematically illustrated in fig. S9. The strain sensor array was then completely picked up using the black polyester thin film–coated TRT (B-TRT) stamp, and Fig. 3B shows the optical image of the strain sensor array
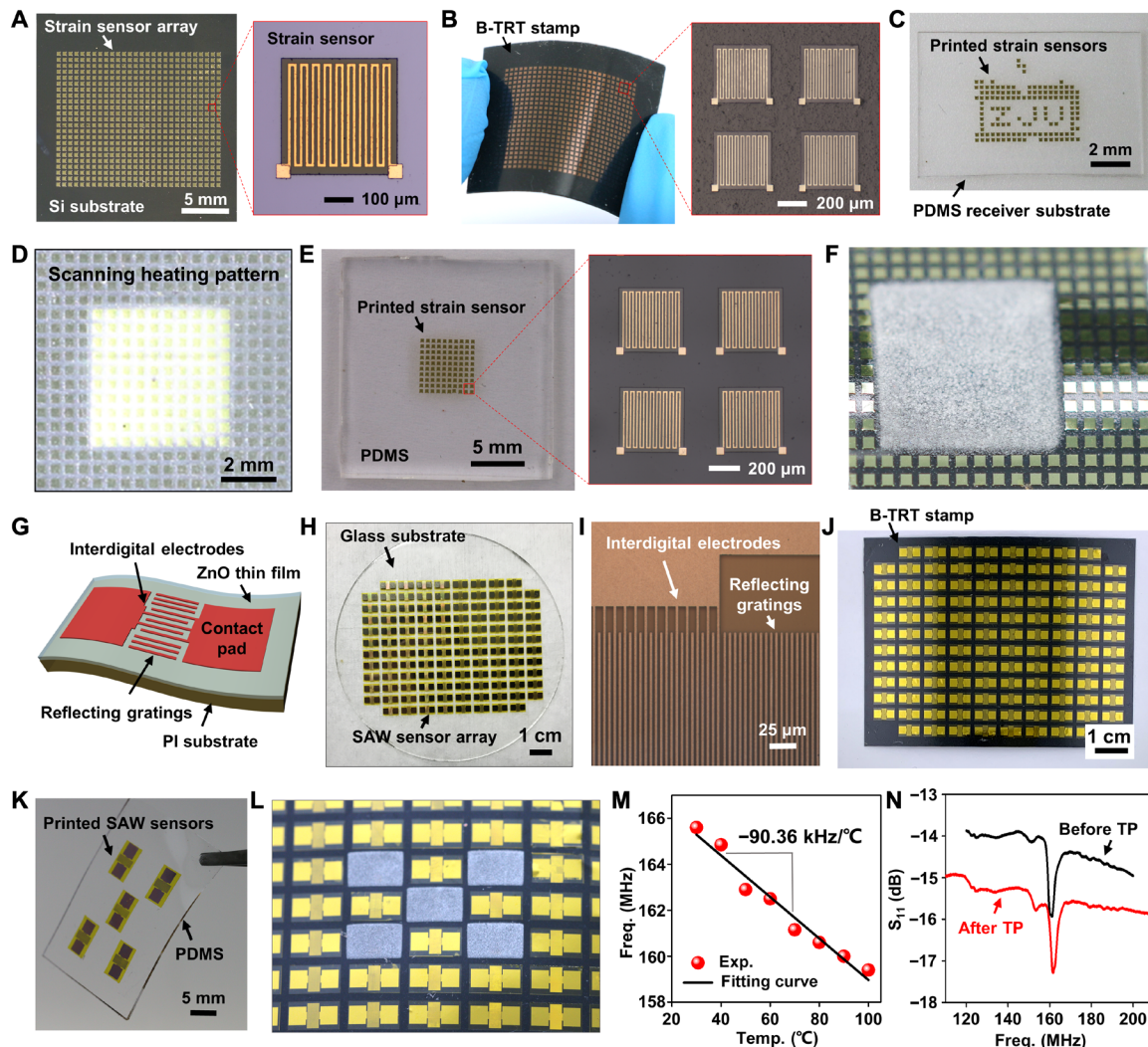
Fig. 3. Programmable and scalable transfer printing in a highthroughput manner via scanning laser beam functionality. Optical images of the flexible strain sensor array (**A**) on fabricated Si substrate and (**B**) on B-TRT stamp, respectively. (**C**) Selectively printed strain sensors on the PDMS substrate. (**D**) Optical image of strain sensors on the B-TRT stamp with a 10 by 10 array heated by the scanning laser beam. Optical images of strain sensors (**E**) printed on the PDMS substrate and (**F**) left on the B-TRT stamp after programmable and scalable transfer printing. (**G**) Schematic layout of ZnO thin film–based flexible SAW sensor. Optical images of flexible SAW sensor array (**H**) on fabricated glass substrate with (**I**) the magnified view of IDTs, and (**J**) on B-TRT stamp. Optical images of the flexible SAW sensors (**K**) printed on the PDMS substrate and (**L**) left on the B-TRT stamp after programmable and scalable transfer printing. The measured resonant frequency of the flexible SAW sensor (**M**) as a function of temperature increase and (**N**) before and after transfer printing on the PDMS substrate at 70°C. Photo credit: C.W., Zhejiang University.

on the B-TRT stamp in deformable form. Here, to demonstrate that the B-TRT stamp is also applicable for selective transfer printing of ultrathin inks via the programmable transfer printing prototype with the automated translational stage shown in fig. S3. We first studied the transfer efficacy of the B-TRT stamp on heating parameters of the localized laser by selective transfer printing of a 3 by 3 array of strain sensors, where all strain sensors except the central one were heated under various heating powers and durations, as shown in fig. S10. It is shown that three repetitive cycles of pulse input can achieve adequate heating of the B-TRT stamp for successful transfer printing of all desired inks, while excessive heating (more than eight cycles) will cause thermal disturbance to neighboring inks due to the heat transfer. Furthermore, more complex patterns such as a television screen–like pattern inspired with Tetris mania that consists of the discrete strain sensors with variable densities can be easily

transfer printed through the programmable heating of the B-TRT stamp where individual strain sensor to be transferred was occupied (fig. S11 and Fig. 3C).

Furthermore, by using the scanning laser beam functionality, the scalable transfer printing of functional inks in a high-throughput manner can be achieved, which remains a difficult challenge for previous transfer printing techniques. To obtain a desired laser power and scanning speed for reliable and high-reliability transfer printing, the surface roughness of the B-TRT stamp under various applied laser powers and scanning speeds was measured after being heated by the scanning laser beam with the same scanning pattern (8-mm by 8-mm square). The optical images of the B-TRT stamp before and after being heated by the scanning laser at a constant scanning speed of 2000 mm/s and applied laser power of 0.588 W are shown in fig. S12 (A and B). The corresponding SEM images

and measured profile (fig. S12C) show the uniform topography across various positions of the B-TRT stamp, similar to these heated on a hotplate, which indicates the feasibility of large-area and selective transfer printing of functional inks via the laser-assisted scanning heating of the B-TRT stamp. Figure 3D shows the optical image of the strain sensor array on the B-TRT stamp with a 5-mm by 5-mm scanning heating square region occupied by a 10 by 10 array of strain sensors heated by scanning laser beam. The scanning speed was set as 2000 mm/s, which takes only 3.72 s to complete the whole scanning process (movie S1), and is highly efficient for large-area and selective transfer printing of functional inks onto various receiver substrates. Figure 3E shows the corresponding optical image of the printed strain sensors of a 10 by 10 array on a PDMS substrate, and no visible damage and undesired disturbance of position were observed from the magnified microscopic image. The optical image of the strain sensors left on the B-TRT stamp after the programmable and scalable transfer printing via the scanning laser beam is shown in Fig. 3F. It is shown that the scanning laser beam can hold high scanning precision and has little thermal transfer effect on adjacent functional inks not to be transferred.

To quantify the effect of the laser-assisted programmable and scalable transfer printing on the performance of functional inks transferred, flexible surface acoustic wave (SAW) devices were fabricated and transfer printed via the scanning laser beam functionality. The schematic image in Fig. 3G highlights the layout of the flexible SAW sensor, which consists of a layer of ZnO piezoelectric thin film on flexible Kapton polyimide substrate, interdigital transducers (IDTs), and reflecting gratings. The resonant frequency of the SAW sensor that is defined by the width and pitch of IDTs under the given thickness of the ZnO thin film is sensitive to the external environment stimuli (e.g., temperature and strain) and can be measured by the network analyzer. Figure 3H shows the optical image of the fabricated wafer-scale flexible SAW sensor array on a 4-inch glass substrate. The fabrication process of the flexible SAW sensor array is illustrated in fig. S13. The magnified microscopic image of IDTs (width and pitch, 2.5 μm) and reflecting gratings are shown in Fig. 3I, which gives the wavelength and corresponding resonant frequency of the SAW sensor of 10 μm and 165.6 MHz at room temperature, respectively. The ZnO piezoelectric thin film that was sputtered on Kapton substrate by direct current (dc) reactive magnetron has substantial effect on the performance of the flexible SAW sensor. Thus, the typical x-ray diffraction spectrum and the cross-sectional SEM image of the ZnO thin film were performed (fig. S14). A large peak at 34.3° was observed, which represents the (0 0 0 2) crystal orientation, similar to these previously deposited on Kapton substrates (39–41). Figure 3J shows the optical image of the wafer-scale SAW sensor array on the B-TRT stamp picked up completely from their fabricated glass substrate. By using the programmable and scalable scanning laser beam functionality, the SAW sensor array attached on the B-TRT stamp can be selectively transfer printed onto a slab of PDMS receiver substrate on demand. Figure 3K shows the optical image of the selectively transfer-printed SAW sensors on a PDMS slab, corresponding to a square scanning heating pattern in fig. S15 and the optical image of the SAW sensors left on the B-TRT stamp after the programmable and scalable transfer printing is shown in Fig. 3L. Flexible SAW devices have wide applications in biochemical sensing (39, 41), microfluidics (40), and substantial advantages in developing wireless and passive sensors (42). Here, the fabricated flexible SAW sensor is sensitive to the temperature change and can be used to monitor the

temperature or respirations of the human body. Figure 3M shows the measured resonant frequency of the flexile SAW sensor as a function of temperature increase, which holds good linear relationship for temperature sensing. The resonant frequency of the fabricated SAW sensor on the glass substrate and PDMS substrate, respectively, was also measured (Fig. 3N). It is observed that the resonant frequency of the SAW sensor has a little shift before and after the programmable transfer printing via the scanning laser beam. However, it will not affect their envisioned applications for biosignals sensing and microfluid actuations since the relationship between the resonant frequency and the sensing environmental factors such as temperature and deformation is more critical for sensing applications, which is basically independent of the small change of the initial resonant frequency. In short, the results here demonstrate the feasibility of the programmable and scalable transfer printing prototype via the scanning laser beam functionality.

Selective transfer printing of ultrathin inorganic μ-LEDs for flexible display

Inorganic microscale LEDs (μ-LEDs) that outperform the organic LEDs in important properties such as brightness, lifetime, and efficiency have enabled a broad spectrum of emerging applications in deformable displays (5, 6, 18–20), wearable optoelectronic sensors (1, 2, 12, 21, 43), and skin phototherapy (44). Here, with the aid of the TRT stamp–based programmable transfer printing prototype, ultrathin μ-LED array–based flexible display can be easily developed in a highly efficient and low-cost manner. To fabricate the ultrathin μ-LED array–based large-area flexible display, the InGaN μ-LED bare dies fabricated on sapphire wafer were first picked up to the TRT stamp by the standard laser liftoff process. The schematic image in fig. S16 shows the main steps to harvest wafer-scale, ultrathin μ-LED bare dies from their native sapphire wafer to the shape-conformal TRT stamp, which involve (i) preparing the InGaN μ-LED bare dies with trench etching on a 4-inch sapphire wafer, (ii) laminating the TRT stamp with μ-LED bare dies on the sapphire wafer, and (iii) picking up the μ-LED bare die array from the sapphire wafer after the laser liftoff process by a commercially available laser liftoff apparatus (DSI-SC8016, Han's Laser Technology Co. Ltd.). It is noted that the process is also applicable for the TRT stamp to harvest other types of tiny, ultrathin, and delicate bare dies or chips from their fabricated wafer in large-area form as long as the bare dies or chips can be adapted to the traditional laser liftoff process.

Figure 4A shows the optical image of the harvested wafer-scale ultrathin, tiny μ-LED bare dies (285 μm by 285 μm by 4.6 μm) on the TRT stamp in a relatively dense form (pitch, 295 μm). The magnified detail of the μ-LED bare die on the TRT stamp is shown in Fig. 1F. By using the programmable transfer printing prototype with the automated translational stage shown in fig. S3, a 10 by 10 array of μ-LED in a sparse form (pitch, 885 μm) was selectively printed onto a temporary PDMS receiver substrate from a myriad of μ-LEDs attached on the TRT stamp. Figure 4B shows the selective transfer printing pattern through the programmable laser heating, and the optical image in Fig. 4C shows the printed μ-LED array on a temporary PDMS receiver substrate with the magnified image on its right hand. To fabricate the ultrathin inorganic μ-LED–based flexible display, a layer of polyimide thin film was first spin coated on a cleaned glass slide (5 cm by 6 cm) and baked on a hotplate at 110°C for 50 s. Then, the printed μ-LED array on the temporary PDMS substrate was transfer printed onto the polyimide iodide (PI)–coated glass substrate
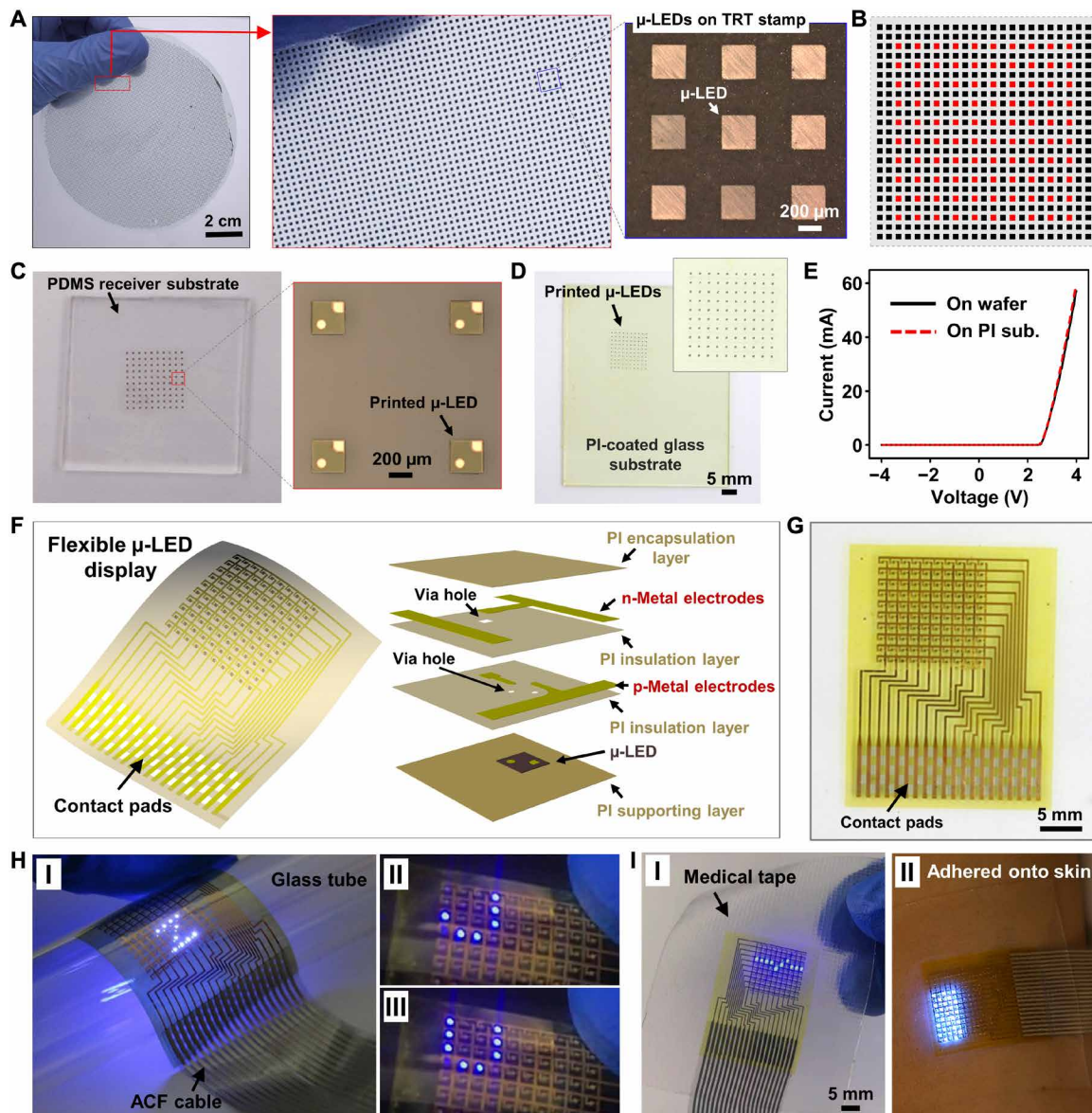
Fig. 4. Transfer-printed ultrathin μ-LED array for flexible display and healthcare. (**A**) Optical image of transferred μ-LEDs on the TRT stamp from the fabricated 4-inch sapphire wafer by the standard laser liftoff process. (**B**) Schematic illustration of selectively transfer printing pattern from dense form on the TRT stamp into sparse array for usage. The red squares indicate the μ-LEDs to be transferred from the TRT stamp. (**C**) Optical image of selectively transfer-printed μ-LEDs in a 10 by 10 array on the PDMS temporary receiver substrate. (**D**) Optical image of μ-LEDs transfer printed onto the polyimide substrate from the PDMS temporary receiver substrate using the TRT stamp. (**E**) I-V curve of the μ-LED on the fabricated sapphire wafer and receiving polyimide substrate, respectively. (**F** and **G**) Schematic and optical images of the fabricated inorganic μ-LED array–based flexible display. (**H**) Optical image of μ-LED array–based flexible display wrapped around a glass tube with displayed letters of ZJU. (**I**) Flexible display attached on the medical tape and mounted onto skin for phototherapy. Photo credit: C.W., Zhejiang University.

with the TRT stamp via the global thermal stimuli on a hotplate (Fig. 4D). To check the optoelectronic performance of the μ-LEDs during the programmable transfer printing process, the I-V characteristic of the μ-LED was measured on the fabricated sapphire wafer and target PI substrate, respectively (Fig. 4E). The consistency of the current-voltage curves indicates that the laser-assisted programmable transfer printing technique in this context has little effect on the performance of the transferred μ-LED bare dies. Owing to the ultrathin feature of the μ-LEDs, it is convenient to assemble the printed μ-LEDs into individually addressable array by using con-

ventional microfabrication process. Figure 4F shows the exploded view of the ultrathin μ-LED–based flexible display, which consists of the ultrathin PI supporting layer, PI insulating layers, and PI encapsulating layer, as well as the n-metal and p-metal interconnects. The detailed fabrication process of the flexible display is described in Materials and Methods and schematically illustrated in fig. S17. The optical image of the fabricated ultrathin μ-LED–based flexible display in 10 by 10 pixels is shown in Fig. 4G, which covers a total in-plane size of 2.19 cm by 2.79 cm and thickness of around 15 μm. The geometry and magnified image of the flexible display are given

in fig. S18. Because of the extraordinary flexibility of the fabricated flexible display, the device can be wrapped around a glass tube (diameter, 20 mm) with displayed patterns, i.e., "Z," "J," and "U" (Fig. 4H), where a soft ACF cable is used to connect the flexible μ-LED display device with the external programmable power supply and software (movie S2). Furthermore, the flexible μ-LED display can be adhered on the medical tape (Silicone adhesion tape, 3M) and then well integrated onto the skin with various patterns displayed (Fig. 4I), which has important applications in wearable displays and phototherapy of psoriasis (44). In addition to the μ-LED assembly, the quantum dot transfer printing can be another potential application of the current technique, which can be even more challenging than a solid film of the same thickness. Some researchers have reported specific transfer printing methods to assemble high-resolution quantum dot display (45, 46).

DISCUSSION

In summary, we presented a simple, cost-effective, yet robust transfer printing technique, which combines the merits of the programmable and scalable assembly capability of tiny, ultrathin, and delicate functional components with high reliability and efficiency. Demonstrations of this protocol involve selective and large-area transfer printing of electronic or optoelectronic components including Si nanomembranes, Si nanomembrane–based photodiodes, and polyimide-based thin film sensors, as well as the manufacturing of ultrathin inorganic LED array–based flexible display. The results reported herein overcome the substantial limits of currently available transfer printing prototypes and imply several impressive consequences. First, the design of in situ actively actuated surface microstructures in this context provides a simple yet robust way to enable strong adhesion for reliable retrieval of inks from fabricated substrates and, simultaneously, weak adhesion for successful release of inks to various receiver substrates through external thermal stimuli. The predefined surface relief microstructures in most previous designs will unexpectedly decrease the adhesion strength of the stamp extremely and lead to low yields for picking up inks from the source wafers. Second, the transfer printing prototype has the ability to release tiny, ultrathin, and delicate functional components in a programmable and scalable manner into spatially organized arrangements with arbitrary layouts from myriads of inks attached on the stamp, which is critically essential to large-area manufacturing of high-performance wearable electronics in a highly efficient and low-cost manner. Together, the innovative transfer printing prototype opens up a simple, cost-effective yet robust route toward large-area integration of ultrathin and delicate functional micro-objects with high yields in a programmable fashion and could create engineering opportunities in widespread applications such as wearable health-monitoring devices, deformable displays, and heterojunction hybrid electronics.

However, there are also several facets that should be improved in the future. One is that the adhesion switch of the TRT stamp needs to be triggered by external temperature (~90°C) through a programmable laser system. Although the temperature is not too high for most functional components, it may cause thermal degradation for certain types of temperature-sensitive devices such as the perovskite-based optoelectronic devices (45, 46). Another is that the current approach is well suitable to transfer components of hundreds of micrometers while it may have difficulty in the transfer printing of smaller functional components with the resolution depending on

the size of expandable microspheres (~45 μm in this work). Thus, the scalable design for the size and shape of expandable microspheres is expected to further widen its utility for smaller and thinner functional components or even nanomaterial assemblies.

MATERIALS AND METHODS
Adhesion strength tests
The energy release rate that is used to quantify the adhesion strength of the TRT stamp was measured at various temperatures by a peeling test apparatus. To prepare the test sample, the TRT stamp was first cut into desired sheet with the size of 1 cm by 10 cm and attached onto a cleaned glass slide. Then, the TRT sheet on the glass slide was mounted on a hotplate and connected to the load cell of tensile and compression tester (Instron 5944). The 90° peeling test was performed at various temperatures at a constant peeling speed of 1000 μm/s to obtain the maximum peeling force. The energy release rate was calculated by averaging the maximum peeling force with TRT sheet width from seven repetitive trials.

Fabrication of ultrathin Si nanomembrane pellet array
To prepare the silicon nanomembrane pellet array, an SOI wafer with 200-nm-thick single crystalline Si on top was cleaned and spin coated with AZ 5214 photoresist at 2000 rpm for 40 s and then baked on a hotplate at 110°C for 60 s. The geometry of the Si square pellet (400 μm by 400 μm) of the 69 by 69 array was defined by ultraviolet photolithography with a dose of 200 mJ cm^{-2}, followed by developing for 50 s by an NMD 2.38% developer. Thereafter, the Si pellet array was patterned by inductively coupled plasma (ICP) etching for 60 s under a sulfur hexafluoride environment [gas flow, 50 standard cubic centimeters per minute (sccm)]. To avoid the floating away of Si pellets after full removal of the buried SiO_2 layer, the photoresist anchors for the Si pellet array were formed by photolithography after etching of exposed SiO_2 buffer layer in buffer oxide etchant (BOE) (6:1). The Si pellet array was lastly separated from the SOI wafer by immersion in the concentrated hydrofluoric acid (49%) for 180 min after full undercut etching of the SiO_2 buffer layer. The fabrication process of the Si pellets with 3-μm thickness follows the similar procedures.

Fabrication of the Si nanomembrane–based photodetector
The fabrication involves selective doping of an SOI wafer with 3-μm-thick top single crystalline silicon (p-type; resistivity, 15 ohm·cm). A layer of SO_2 (800 nm) was first deposited by plasma-enhanced chemical vapor deposition onto the cleaned SOI wafer (2.5 cm by 2.5 cm) to form a diffusion mask for n-dopant. The doping windows were defined by photolithography and wet etching in BOE (1:6) for 5 min. The phosphorous-based spin-on-dopant (Phosphorous, PDC5-2500, Futurrex) was then spin coated at 4000 rmp for 60 s and dried in air for 10 min. Then, two coated samples with coated sides were placed to face each other and baked on a hotplate at 200°C for 60 s, followed by annealing at 950°C for 5 min at N_2 flow of 80 sccm to form two back-to-back p-n diodes. The photodetector array was patterned and released from the Si wafer by following the same procedures for the Si nanomembrane pellet array aforementioned.

Fabrication of flexible strain sensor array
To prepare the strain sensor array, a thin layer of SiO_2 (300 nm thick) was first deposited onto a cleaned 4-inch silicon wafer. Then, the polyimide precursor (ZKPI-305IIE, POME) was spin coated at 2000 rpm

for 60 s and cured on a hotplate at 80°C for 60 min, 110°C for 60 min, and 230°C for 120 min, respectively. The metal layers (Cr/Au, 5 nm/150 nm) were then deposited on the polyimide layer by an e-Beam evaporator and patterned through ultraviolet lithography and the liftoff process. Thereafter, another layer of polyimide as encapsulation was formed, and the whole bilayer polyimide film was patterned by ICP to obtain strain sensor array. Last, the strain sensor array was connected by photoresist anchors and released from the Si substrate by immersion in BOE (1:6). The released strain sensor array was then held with a PDMS-coated glass slide and picked up using the B-TRT stamp for transfer printing after removal of the photoresist anchors with acetone.

Fabrication of flexible SAW sensor array
To fabricate the flexible SAW sensors, a Kapton polyimide film of 25-μm thickness was laminated onto a PDMS-coated glass slide to serve as the substrate due to its excellent flexibility, chemical stability, and wide operating temperature range. As previously reported, a ZnO piezoelectric thin film was deposited on the Kapton film by dc reactive magnetron at a mixture of Ar and O_2 with 100 and 50 sccm flow rates, and constant deposition temperature and pressure, i.e., 200°C and 2 Pa, respectively. The bias voltage at metallic Zn target (99.99% purity and 100 mm diameter) and applied power during deposition were set as 75 V and 175 W, respectively, to yield a layer of ZnO with ~3-μm thickness at a deposition rate of 0.5 μm/hour. The interdigitated transducer electrodes and reflecting gratings (Al, 100-nm thick) were fabricated by standard ultraviolet photolithography and electronic beam (e-beam) evaporation, followed by the liftoff process to define the wavelength of the SAW sensor of 10 μm and corresponding resonant frequency of ~165.66 MHz at room temperature. The ZnO piezoelectric thin film was patterned by wet etching in dilute HCl solution (1:10). Thereafter, a layer of PMMA was spin coated on top of SAW sensors for temporary protecting. The Kapton film was cut into desired rectangular size (7 mm by 4 mm) to form SAW sensor array and picked up using the B-TRT stamp for transfer printing.

Fabrication of flexible μ-LED display
To fabricate the μ-LED array–based flexible display, μ-LED array was selectively transfer printed onto a PDMS slab by the programmable transfer printing prototype. Then, the polyimide precursor (ZKPI 305IIE, POME) was spin coated onto a cleaned glass slide at 4000 rpm for 60 s and baked on a hotplate at 110°C for 50 s. The printed μ-LED array on the PDMS slab was picked up using the TRT stamp and transfer printed again onto the PI substrate after heating on hotplate at 90°C for 40 s to release the adhesion of the TRT stamp. Thereafter, the PI substrate was baked on a hotplate at 80°C for 60 min, 110°C for 60 min, and 230°C for 120 min, respectively. The polyimide precursor (ZKPI 305IID, POME) was spin coated at 2000 rpm for 60 s and baked on a hotplate to form an insulating layer and followed with ultraviolet lithography and ICP etching to create via holes for metal interconnect. Cr and Au metal layers (10 and 400 nm, respectively) were deposited and patterned by photolithography and the liftoff process to form p-metal interconnect. Another layer of PI thin film (ZKPI 305IID, POME) was spin coated at 2000 rpm for 60 s and baked to form an insulating layer and followed with ICP etching to create via holes for n-metal interconnect. Then, Cr and Au metal layers (10 and 400 nm) were deposited and patterned by photolithography and the liftoff process to form n-metal interconnect.

Last, another layer of PI thin film (ZKPI 305IIE, POME) was spin coated at 2000 rpm for 60 s and baked to form an encapsulating layer. The shapes of the flexible μ-LED display device and contact pads were defined by ICP etching of the whole PI layer with patterned Al as etching mask. The device was released from the glass slide by immersion in BOE.

SUPPLEMENTARY MATERIALS
Supplementary material for this article is available at http://advances.sciencemag.org/cgi/content/full/6/25/eabb2393/DC1

REFERENCES AND NOTES
1. T.-i. Kim, J. G. McCall, Y. H. Jung, X. Huang, E. R. Siuda, Y. Li, J. Song, Y. M. Song, H. A. Pao, R.-H. Kim, C. Lu, S. D. Lee, I.-S. Song, G. Shin, R. Al-Hasani, S. Kim, M. P. Tan, Y. Huang, F. G. Omenetto, J. A. Rogers, M. R. Bruchas, Injectable, cellular-scale optoelectronics with applications for wireless optogenetics. *Science* **340**, 211–216 (2013).
2. A. D. Mickle, S. M. Won, K. N. Noh, J. Yoon, K. W. Meacham, Y. Xue, L. A. McIlvried, B. A. Copits, V. K. Samineni, K. E. Crawford, D. H. Kim, P. Srivastava, B. H. Kim, S. Min, Y. Shiuan, Y. Yun, M. A. Payne, J. Zhang, H. Jang, Y. Li, H. H. Lai, Y. Huang, S.-I. Park, R. W. Gereau IV, J. A. Rogers, A wireless closed-loop system for optogenetic peripheral neuromodulation. *Nature* **565**, 361–365 (2019).
3. C. Dagdeviren, B. D. Yang, Y. Su, P. L. Tran, P. Joe, E. Anderson, J. Xia, V. Doraiswamy, B. Dehdashti, X. Feng, B. Lu, R. Poston, Z. Khalpey, R. Ghaffari, Y. Huang, M. J. Slepian, J. A. Rogers, Conformal piezoelectric energy harvesting and storage from motions of the heart, lung, and diaphragm. *Proc. Natl. Acad. Sci. U.S.A.* **111**, 1927–1932 (2014).
4. D.-H. Kim, N. Lu, R. Ma, Y.-S. Kim, R.-H. Kim, S. Wang, J. Wu, S. M. Won, H. Tao, A. Islam, K. J. Yu, T.-i. Kim, R. Chowdhury, M. Ying, L. Xu, M. Li, H.-J. Chung, H. Keum, M. McCormick, P. Liu, Y.-W. Zhang, F. G. Omenetto, Y. Huang, T. Coleman, J. A. Rogers, Epidermal electronics. *Science* **333**, 838–843 (2011).
5. Y. M. Song, Y. Xie, V. Malyarchuk, J. Xiao, I. Jung, K. J. Choi, Z. Liu, H. Park, C. Lu, R. H. Kim, R. Li, K. B. Crozier, Y. Huang, J. A. Rogers, Digital cameras with designs inspired by the arthropod eye. *Nature* **497**, 95–99 (2013).
6. S. I. Park, Y. Xiong, R.-H. Kim, P. Elvikis, M. Meitl, D.-H. Kim, J. Wu, J. Yoon, C.-J. Yu, Z. Liu, Y. Huang, K.-c. Hwang, P. Ferreira, X. Li, K. Choquette, J. A. Rogers, Printed assemblies of inorganic light-emitting diodes for deformable and semitransparent displays. *Science* **325**, 977–981 (2009).
7. H.-s. Kim, E. Brueckner, J. Song, Y. Li, S. Kim, C. Lu, J. Sulkin, K. Choquette, Y. Huang, R. G. Nuzzo, J. A. Rogers, Unusual strategies for using indium gallium nitride grown on silicon (111) for solid-state lighting. *Proc. Natl. Acad. Sci. U.S.A.* **108**, 10072–10077 (2011).
8. B. Peng, Y. Huang, Z. Yin, Y. Xiong, Analysis of interfacial peeling in IC chip pick-up process. *J. Appl. Phys.* **110**, 073508 (2011).
9. Z. Liu, Y. Huang, J. Chen, Z. Yin, Tunable peeling technique and mechanism of thin chip from compliant adhesive tapes. *IEEE Trans. Compon. Packag. Manuf. Technol.* **4**, 560–568 (2014).
10. A. Carlson, A. M. Bowen, Y. Huang, R. G. Nuzzo, J. A. Rogers, Transfer printing techniques for materials assembly and micro/nanodevice fabrication. *Adv. Mater.* **24**, 5284–5318 (2012).
11. C. Linghu, S. Zhang, C. Wang, J. Song, Transfer printing techniques for flexible and stretchable inorganic electronics. *npj Flexible Electron.* **2**, 26 (2018).
12. E. Song, C.-H. Chiang, R. Li, X. Jin, J. Zhao, M. Hill, Y. Xia, L. Li, Y. Huang, S. M. Won, K. J. Yu, X. Sheng, H. Fang, M. A. Alam, Y. Huang, J. Viventi, J.-K. Chang, J. A. Rogers, Flexible electronic/optoelectronic microsystems with scalable designs for chronic biointegration. *Proc. Natl. Acad. Sci. U.S.A.* **116**, 15398–15406 (2019).
13. J. Yoon, S.-M. Lee, D. Kang, M. A. Meitl, C. A. Bower, J. A. Rogers, Heterogeneously integrated optoelectronic devices enabled by micro-transfer printing. *Adv. Opt. Mater.* **3**, 1313–1335 (2015).
14. M. A. Meitl, Z.-T. Zhu, V. Kumar, K. J. Lee, X. Feng, Y. Y. Huang, I. Adesida, R. G. Nuzzo, J. A. Rogers, Transfer printing by kinetic control of adhesion to an elastomeric stamp. *Nat. Mater.* **5**, 33–38 (2006).
15. H. Luo, C. Wang, C. Linghu, K. Yu, C. Wang, J. Song, Laser-driven programmable non-contact transfer printing of objects onto arbitrary receivers via an active elastomeric micro-structured stamp. *Natl. Sci. Rev.* **7**, 296–304 (2020).
16. A. Carlson, S. Wang, P. Elvikis, P. M. Ferreira, Y. Huang, J. A. Rogers, Active, programmable elastomeric surfaces with tunable adhesion for deterministic assembly by transfer printing. *Adv. Funct. Mater.* **22**, 4476–4484 (2012).
17. S. Kim, J. Wu, A. Carlson, S. H. Jin, A. Kovalsky, P. Glass, Z. Liu, N. Ahmed, S. L. Elgan, W. Chen, P. M. Ferreira, M. Sitti, Y. Huang, J. A. Rogers, Microstructured elastomeric surfaces with reversible adhesion and examples of their use in deterministic assembly by transfer printing. *Proc. Natl. Acad. Sci. U.S.A.* **107**, 17095–17100 (2010).

18. H. E. Lee, J. H. Shin, J. H. Park, S. K. Hong, S. H. Park, S. H. Lee, J. H. Lee, I.-S. Kang, K. J. Lee, Micro light-emitting diodes for display and flexible biomedical applications. *Adv. Funct. Mater.* **29**, 1808075 (2019).

19. M. A. Meitl, E. Radauscher, R. Rotzoll, B. Raymond, S. Bonafede, D. Gomez, T. Moore, C. Prevatte, A. I. M. Fecioru, A. J. Trindade, C. A. Bower, 19-4:*Invited Paper*: emissive displays with transfer-printed microscale inorganic LEDs. *SID Symp. Dig. Tech. Pap.* **48**, 257–263 (2017).

20. V. R. Marinov, 52-4: Laser-enabled extremely-high rate technology for μLED assembly. *SID Symp. Dig. Tech. Pap.* **49**, 692–695 (2018).

21. J. Kim, P. Gutruf, A. M. Chiarelli, S. Y. Heo, K. Cho, Z. Xie, A. Banks, S. Han, K.-I. Jang, J. W. Lee, K.-T. Lee, X. Feng, Y. Huang, M. Fabiani, G. Gratton, U. Paik, J. A. Rogers, Miniaturized battery-free wireless systems for wearable pulse oximetry. *Adv. Funct. Mater.* **27**, 1604373 (2017).

22. N. Ahmed, C. Dagdeviren, J. A. Rogers, P. M. Ferreira, Active polymeric composite membranes for localized actuation and sensing in microtransfer printing. *J. Micro Syst.* **24**, 1016–1028 (2015).

23. C. Linghu, C. Wang, N. Cen, J. Wu, Z. Lai, J. Song, Rapidly tunable and highly reversible bio-inspired dry adhesion for transfer printing in air and a vacuum. *Soft Matter* **15**, 30–37 (2019).

24. R. Saeidpourazar, M. D. Sangid, J. A. Rogers, P. M. Ferreira, A prototype printer for laser driven micro-transfer printing. *J. Manuf. Process.* **14**, 416–424 (2012).

25. Y. Gao, Y. Li, R. Li, J. Song, An accurate thermomechanical model for laser-driven microtransfer printing. *J. Appl. Mech. Trans.* **84**, 064501 (2017).

26. J. Bian, L. Zhou, X. Wan, C. Zhu, B. Yang, Y. Huang, Laser transfer, printing, and assembly techniques for flexible electronics. *Adv. Electron. Mater.* **5**, 1800900 (2019).

27. J. Bian, L. B. Y. Zhou, X. D. Wan, M. X. Liu, C. Zhu, Y. A. Huang, Z. P. Yin, Experimental study of laser lift-off of ultra-thin polyimide film for flexible electronics. *Sci. China Technol. Sci.* **62**, 233–242 (2019).

28. Y. Huang, N. Zheng, Z. Cheng, Y. Chen, B. Lu, T. Xie, X. Feng, Direct laser writing-based programmable transfer printing via bioinspired shape memory reversible adhesive. *ACS Appl. Mater. Interfaces* **8**, 35628–35633 (2016).

29. J. Eisenhaure, S. Kim, Laser-driven shape memory effect for transfer printing combining parallelism with individual object control. *Adv. Mater. Tech.* **1**, 1600098 (2016).

30. A. Miriyev, K. Stack, H. Lipson, Soft material for soft actuators. *Nat. Commun.* **8**, 596 (2017).

31. M. Jonsson, O. Nordin, E. Malmström, C. Hammer, Suspension polymerization of thermally expandable core/shell particles. *Polymer* **47**, 3315–3324 (2006).

32. H. Yi, M. Seong, K. Sun, I. Hwang, K. Lee, C. Cha, T.-i. Kim, H. E. Jeong, Wet-responsive, reconfigurable, and biocompatible hydrogel adhesive films for transfer printing of nanomembranes. *Adv. Funct. Mater.* **28**, 1706498 (2018).

33. X. Liu, C. Steiger, S. Lin, G. A. Parada, J. Liu, H. F. Chan, H. Yuk, N. V. Phan, J. Collins, S. Tamang, G. Traverso, X. Zhao, Ingestible hydrogel device. *Nat. Commun.* **10**, 493 (2019).

34. A. Murata, T. Oshima, Y. Arimitsu, K. Kiuchi, *U.S. Patent* 6998175.

35. D. S. Wie, Y. Zhang, M. K. Kim, B. Kim, S. Park, Y. J. Kim, P. P. Irazoqui, X. Zheng, B. Xu, C. H. Lee, Wafer-recyclable, environment-friendly transfer printing for large-scale thin-film nanoelectronics. *Proc. Natl. Acad. Sci. U.S.A.* **115**, E7236–E7244 (2018).

36. S. Bae, H. Kim, Y. Lee, X. Xu, J.-S. Park, Y. Zheng, J. Balakrishnan, T. Lei, H. Ri Kim, Y. I. Song, Y.-J. Kim, K. S. Kim, B. Özyilmaz, J.-H. Ahn, B. H. Hong, S. Iijima, Roll-to-roll production of 30-inch graphene films for transparent electrodes. *Nat. Nanotechnol.* **5**, 574–578 (2010).

37. C. H. Lee, D. R. Kim, X. Zheng, Fabricating nanowire devices on diverse substrates by simple transfer-printing methods. *Proc. Natl. Acad. Sci. U.S.A.* **107**, 9950–9955 (2010).

38. Z. Yan, T. Pan, M. Xue, C. Chen, Y. Cui, G. Yao, L. Huang, F. Liao, W. Jing, H. Zhang, M. Gao, D. Guo, Y. Xia, Y. Lin, Thermal release transfer printing for stretchable conformal bioelectronics. *Adv. Sci.* **4**, 1700251 (2017).

39. H. Jin, X. Tao, S. Dong, Y. Qin, L. Yu, J. Luo, M. J. Deen, Flexible surface acoustic wave respiration sensor for monitoring obstructive sleep apnea syndrome. *J. Micromech. Microeng.* **27**, 115006 (2017).

40. H. Jin, J. Zhou, X. He, W. Wang, H. Guo, S. Dong, D. Wang, Y. Xu, J. Geng, J. K. Luo, W. I. Milne, Flexible surface acoustic wave resonators built on disposable plastic film for electronics and lab-on-a-chip applications. *Sci. Rep.* **3**, 2140 (2013).

41. W. P. Xuan, M. He, N. Meng, X. He, W. Wang, J. Chen, T. Shi, T. Hasan, Z. Xu, Y. Xu, J. K. Luo, Fast response and high sensitivity ZnO/glass surface acoustic wave humidity sensors using graphene oxide sensing layer. *Sci. Rep.* **4**, 7206 (2015).

42. G. M. Ma, Z. Wu, H.-y. Zhou, J. Jiang, W. Chen, S.-S. Zheng, C.-R. Li, X. Li, Z.-b. Wang, A wireless and passive online temperature monitoring system for GIS based on surface-acoustic-wave sensor. *IEEE Trans. Power Deliv.* **31**, 1270–1280 (2016).

43. H. E. Lee, J. Choi, S. H. Lee, M. Jeong, J. H. Shin, D. J. Joe, D. Kim, C. W. Kim, J. H. Park, J. H. Lee, D. Kim, C.-S. Shin, K. J. Lee, Monolithic flexible vertical GaN light-emitting diodes for a transparent wireless brain optical stimulator. *Adv. Mater.* **30**, 1800649 (2018).

44. P. Zhang, M. X. Wu, A clinical review of phototherapy for psoriasis. *Laser Med. Sci.* **33**, 173–180 (2018).

45. T.-H. Kim, D.-Y. Chung, J. Ku, I. Song, S. Sul, D.-H. Kim, K.-S. Cho, B. L. Choi, J. M. Kim, S. Hwang, K. Kim, Heterogeneous stacking of nanodot monolayers by dry pick-and-place transfer and its applications in quantum dot light-emitting diodes. *Nat. Commun.* **4**, 2637 (2013).

46. M. K. Choi, J. Yang, K. Kang, D. C. Kim, C. Choi, C. Park, S. J. Kim, S. I. Chae, T.-H. Kim, J. H. Kim, T. Hyeon, D.-H. Kim, Wearable red-green-blue quantum dot light-emitting diode array using high-resolution intaglio transfer printing. *Nat. Commun.* **6**, 7149 (2015).

Citation: C. Wang, C. Linghu, S. Nie, C. Li, Q. Lei, X. Tao, Y. Zeng, Y. Du, S. Zhang, K. Yu, H. Jin, W. Chen, J. Song, Programmable and scalable transfer printing with high reliability and efficiency for flexible inorganic electronics. *Sci. Adv.* **6**, eabb2393 (2020).